Supplement of Biogeosciences, 21, 3537–3550, 2024
https://doi.org/10.5194/bg-21-3537-2024-supplement

Biogeosciences Open Access EGU

Supplement of

From Iron Curtain to green belt: shift from heterotrophic to autotrophic nitrogen retention in the Elbe River over 35 years of passive restoration

Alexander Wachholz et al.

Correspondence to: Alexander Wachholz (alexander.wachholz@uba.de)

S1. Segment geometry estimation

a. Travel time model

We employ the travel time model introduced by Scharfe et al. (2009) to estimate the travel time (τ) in the Elbe River:

(I) $$\tau(t) = \frac{Q_{ref}}{Q(t)}^{\frac{\tau_{ref.}}{3}}$$

where Q_{ref} is 270 m^3/s, and τ_{ref} is 240 hours. While this model was developed for the entire German Elbe (585 km), we assume the flow velocity is distributed homogeneously and adjust it for the length of our segment (111 km).

b. Channel area model

To predict channel area (*A*), we use a power law relationship, $A(t) = aQ(t)^b$, between discharge (*Q*) and channel area (Booker and Dunbar, 2008). To parameterize this relationship, we apply the Normalized Difference Water Index (NDWI) algorithm (Gao, 1996) on Sentinel 2 images with a 10-meter resolution, taken during various discharge conditions (186-1020 $m^3\ s^{-1}$) and with a maximum of 10% cloud cover over the study area.

c. Channel depth model

To predict channel depth (Z), we also use a power law relationship of the form $Z(t)=aQ(t)^b$ (Modi et al., 2022). We fit the parameters based on data from the Elbe (Aberle et al., 2010).

S2. Gaussian error propagation

We use gaussian error propagation to quantify the uncertainty for the mass balance estimates

(II) $$\sigma_{R_{obs}} = \sqrt{\sigma_{Lin}^2 + \sigma_{Lout}^2}$$

where σ is the absolute error of any term. The errors in L result from the errors in C and Q

(III) $$\sigma_L = \sqrt{\sigma_C^2 Q^2 + \sigma_Q^2 C^2}$$

for σ_C and σ_Q we assume a constant value of 10 % of the current C or Q value. We did not assess R_{obs} on days where Q was larger than the 90th flow percentile or where $\frac{Q_{in} - Q_{out}}{Q_{in}}$ was larger than 0.05 (18 % of all days). This led to an exclusion of 18 % of all dates, most of which (84%) occurred during high flows winter.

S3. Interpolation of hourly dissolved oxygen time series

As daily DO curves are usually sinusoidal (Correa-González et al., 2014) and data from the Elbe confirms this general assumption (Kamjunke et al., 2021; their Fig. 5) we use a sine wave based approach to interpolate hourly DO concentrations from observed daily minimum, maximum, and mean values. We use a sine wave of the form

(IV) $$y(x) = mean + amplitude * \cos\left(\frac{2\pi}{period}(x - phase)\right)$$

and base the parameters *mean*, *amplitude*, *period* (τ), and *phase* (ϕ) on the measured DO concentrations

(V)

$$DO(hour) = DO_{mean}(day) + \frac{DO_{max}(day) - DO_{min}(day)}{2} \cos\left(\frac{2\pi}{\tau(day)}\left(hour - \frac{\phi(day)}{24}\tau(day)\right)\right)$$

where τ is the period of the sine chosen to satisfy that $\tau/2$ is the time between the peak (ϕ) and low (ψ) of DO concentrations. ϕ and ψ, however, are only available for 25 % of all days (n≈2000), so we derived transfer functions (Fig. S6a, b) that estimates τ and ϕ for each day of the year based on daylight hours (time between sunrise and sunset).

(VI) $$\tau(day) = 2(i + m * daylight hours)$$

As ϕ follows a sinusoidal curve itself during the year, we approximate it using a sine function

(VII) $$\phi(day) = 16 + 2\cos\frac{2\pi}{365}(\text{day-}180))$$

This approach leads to dates where the period of the sine τ is less than 24 hours (especially during winter), which means less than 24 hours of DO concentrations are simulated. We use linear interpolation for missing hours, filling a maximum of 12 consecutive hours. We validate this approach by comparing the simulated hourly DO concentrations with 2 years (2015, 2016) high frequency (30-minute) sensor measurements from the same site (Fig. S7) provided by the Niedersächsischer Landesbetrieb für Wasserwirtschaft, Küsten- und Naturschutz (NLWKN).

S4. Metabolism model

S4.1 k600 Estimation

We estimated gross primary production (*GPP*) and ecosystem respiration (*ER*) using a maximum likelihood estimation (*mle*) method (e.g., Richardson et al., 2017). We estimated the gas exchange velocity (k600) using a hydraulically based equation from Raymond et al. (2012, their table 2, model equation 7)

(VIII) $$k_{600} = a\left(V_f S\right)^b Q^{-c} D^d$$

where a, b, c, and d, are the parameters fitted by Raymond et al., (2012), V_f is the flow velocity [m s^{-1}], S is the segment slope [m m^{-1}], Q is discharge [m^3 s^{-1}] and D is the depth [m]. We calculate the flow velocity V_f by dividing the segment length (110 km) by the travel time (estimated as described in Section S1). The resulting distribution of k600 values is shown in figure S8.

S4.2 Estimation of parameter uncertainties

To estimate the uncertainty in the parameters k600, DO_{max} and T_{water} of equation IV, we assess their daily variability using different methods. In case of T_{water}, we use daily minimal and maximal water temperatures which are available from the site Schnakenburg for 20 years. For each day, we then estimate the standard deviation σ_{Twater} around the mean. Finding σ_{Twater} is highly correlated with the day of the year, we use a sine model esitmating its value for each day of the year (Figure S9). For DO_{ma}, the dissolved oxygen concentration at saturation, we propagate σ_{Twater} into the calculation of the dissolved oxygen saturation (as described in Section 2.6) and model the resulting σ_{DOmax} values again as a function of the day of the year (Figure S9). For k600, we have no data available and so use the parameter uncertainty presented in Raymond et al., 2012 to estimate a daily standard deviation of k600, which we simplify by modeling as an exponential function based on discharge (Figure S9).

To assess the sensitivity of using the MLE approach to estimate GPP and ER

towards those uncertainties, we calculate the changes in GPP and ER by adding and subtracting σ_{Twater}, σ_{DOmax} and k600 to the daily assumed values (Fig S11). This analysis does not consider critical parameter combinations (e.g. high k600, high T_{water}) nor does it capture the entire input parameter space. However, it reveals the high importance of k600 for both ER and GPP estimates.

S4.3 Areal extent of the metabolic signal An important consideration when interpreting metabolic estimates is the areal extent over which the single station method integrates. Following Chapra and Di Toro (1991), this can be estimated as follows

(IX) $$ae = \frac{3v}{k600\,z}$$

where v is the flow velocity [m d^{-1}], *k600* is the gas exchange coefficient [m d^{-1}] and z is the channel depth [m]. By using median the median flow velocity (74.000 m d^{-1}), median k600 (2.9 m d^{-1}), and median channel depth (2.8 m), we arrive at an areal extent of 196 km covered by this approach, which is 76 % longer than the investigated segment. However, Kamjunke et al. (2022) showed that ER and NPP rates did change relatively little during the last 200 km of the Elbe compared to its entire length during periods of high biological activity, so we assume the single station metabolism estimation reflects the spatial scale of the DIN balance.

S5. Figures

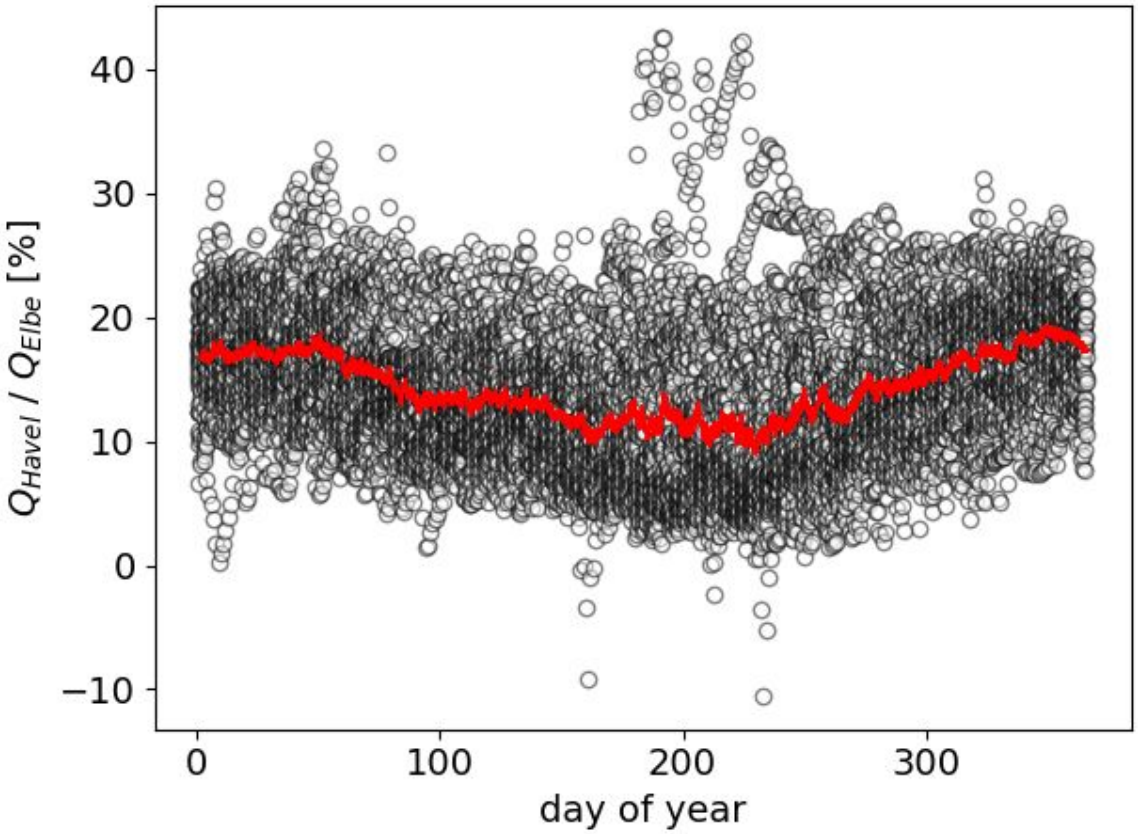

Figure S1. Fraction of the Havels (Gage: Havelberg-Stadt) discharge divided by the discharge of the Elbe (Gage: Neu-Darchau) (Fig.1a, b). Circles show raw data, and the red line is the multi-year mean for each day.

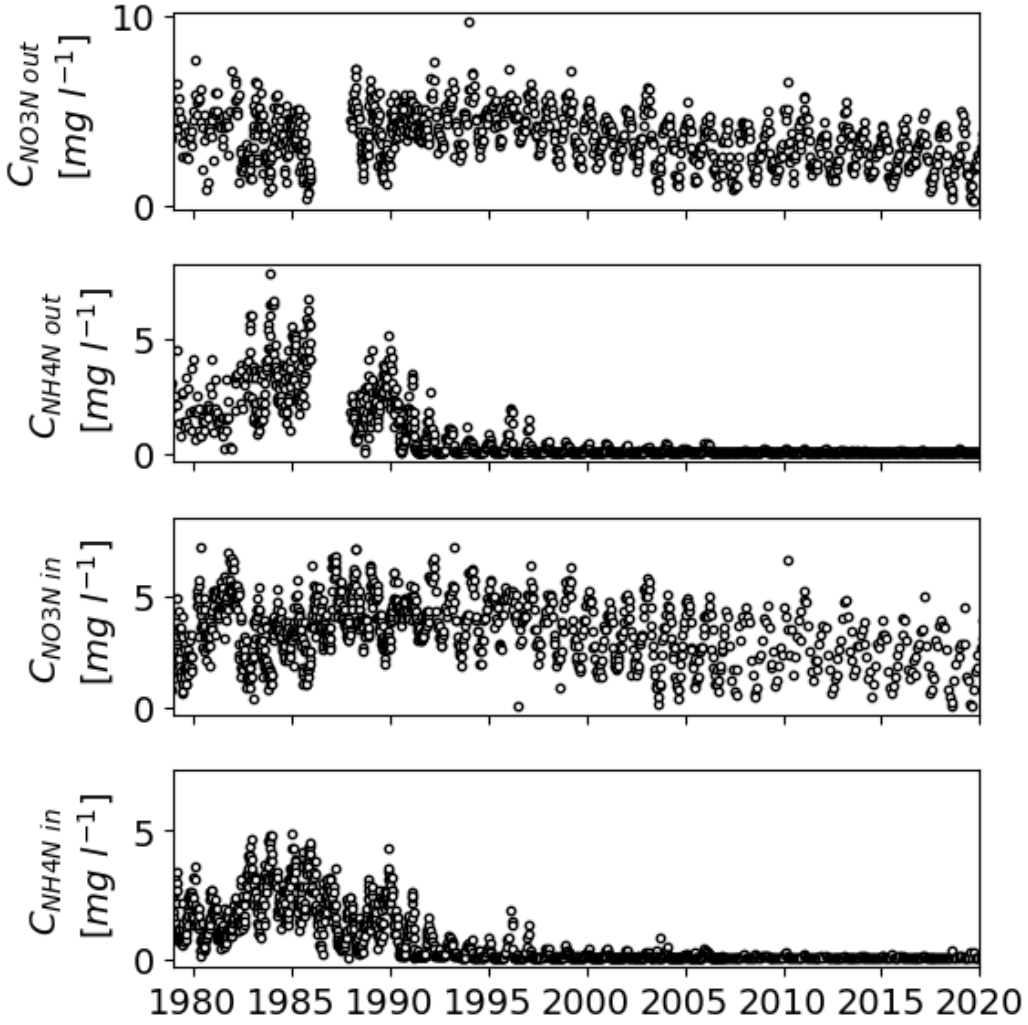

Figure S2: Unprocessed time series of nitrate-N and ammonium-N concentrations at the input sampling site (in) and output sampling site (out) of the two-station mass balance.

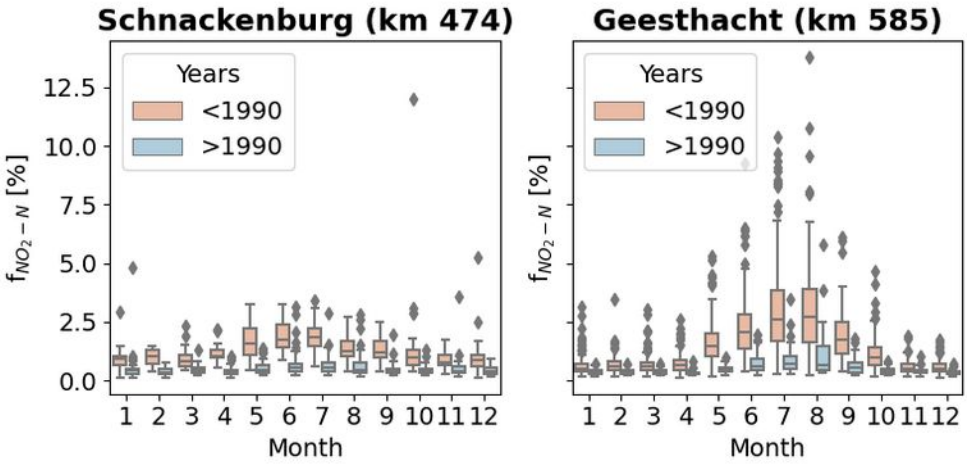

Figure S3: Fraction of NO2-N from dissolved inorganic DIN for the input (Schnackenburg) and output (Geesthacht) sampling sites of the mass balance in %.

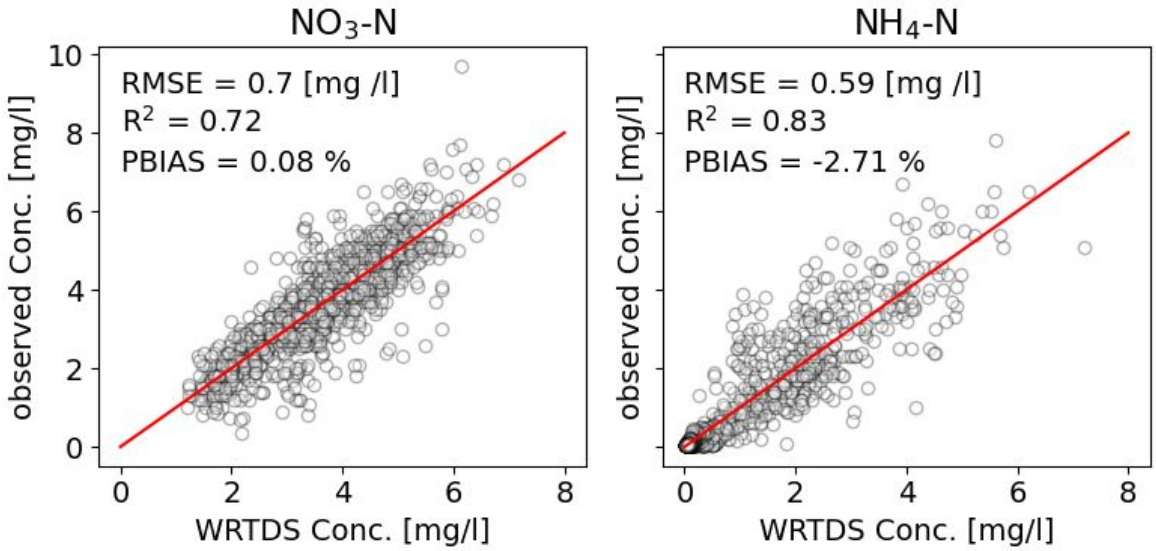

Figure S4: Measured vs WRTDS simulated daily N concentrations for the Elbe at the outlet of the investigated river segment (Geesthacht).

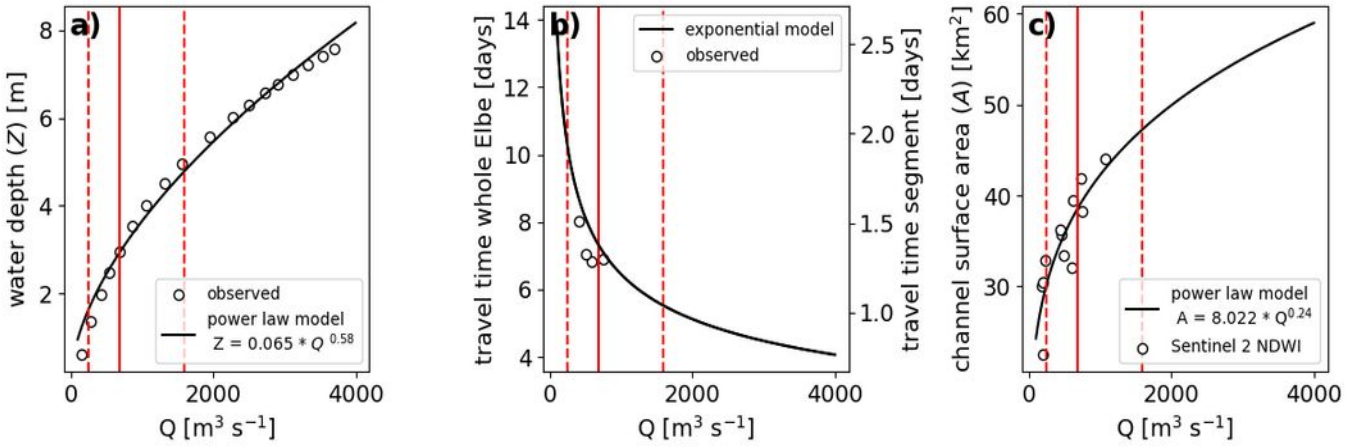

Figure S5. The discharge-based transfer function for channel depth, travel time, and channel surface area. The dashed red lines show the 5th and the 95th, and the solid red line shows the 50th flow percentile for the period 1978-2021 from the Gage Neu Darchau. In panel b), both the travel time along the entire Elbe (left y-axis) and the travel time along the investigated segment (right y-axis) are shown.

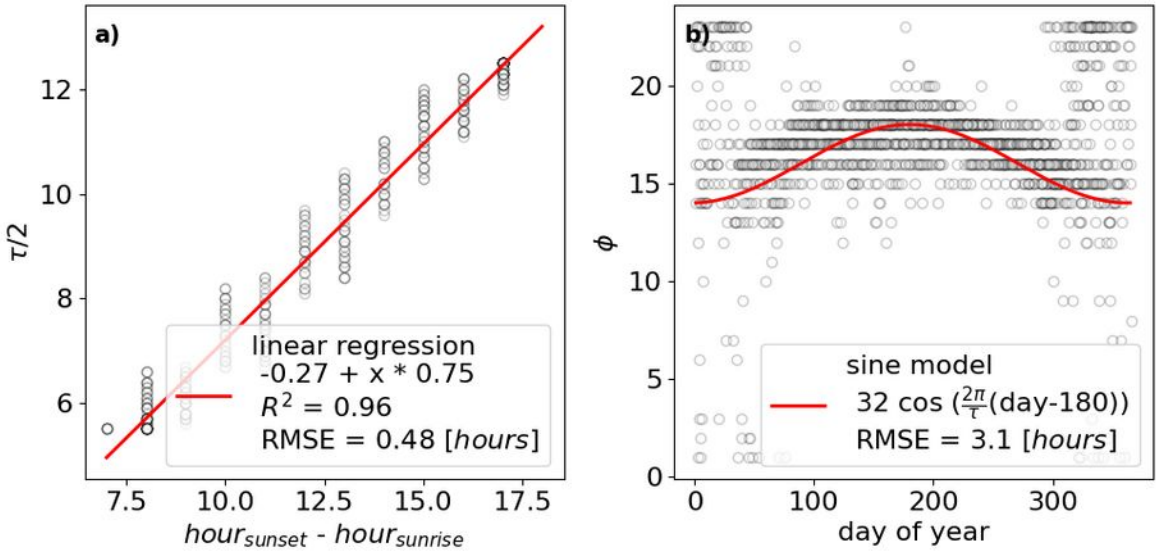

Figure S6. a) Transfer function to predict the time between dissolved oxygen (DO) minimum and maximum (τ/2) based on the hours between sunrise and sunset. b) Transfer function to predict the hour of maximum DO concentrations (ϕ) as a function of the day of the year. Circles show raw data from ~2000 days.

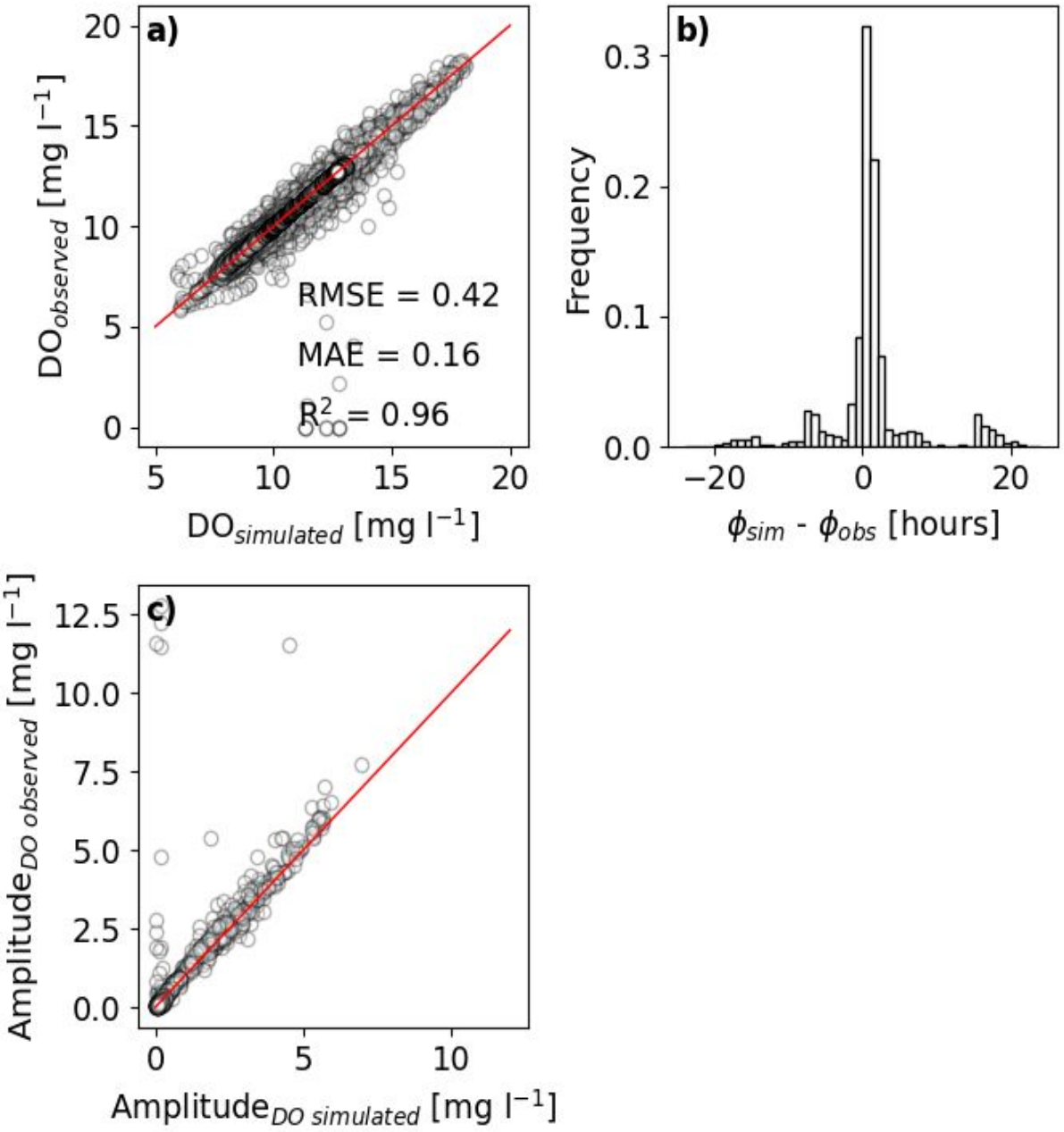

Figure S7. a) Scatter plot between predicted and observed 30 minute dissolved oxygen (DO) concentrations (aggreated to one hour) with the goodness of fit metrics root mean square error (RMSE), mean absolute error (MAE), and correlation coefficient R2. The red line represents a perfect correlation. b) Histogram of the differences between simulated and observed hour of the day with maximum DO concentrations (ϕ). c) Scatter plot between predicted and observed daily amplitude of DO. The red line represents a perfect correlation.

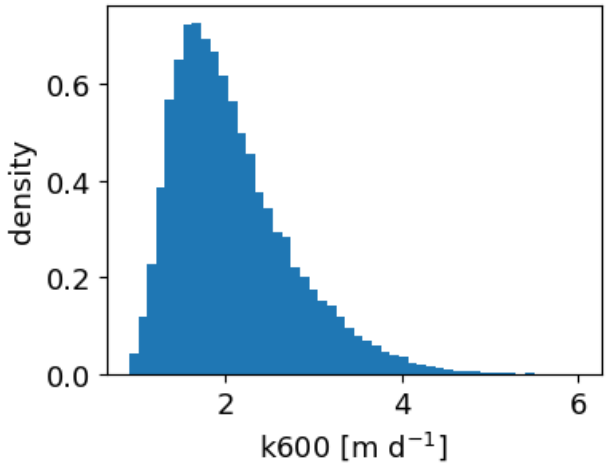

Figure S8 Distribution of simulation gas exchange coeffcient for oxygen (k600) after Raymond et al., 2012 (their table 2, equation 7).

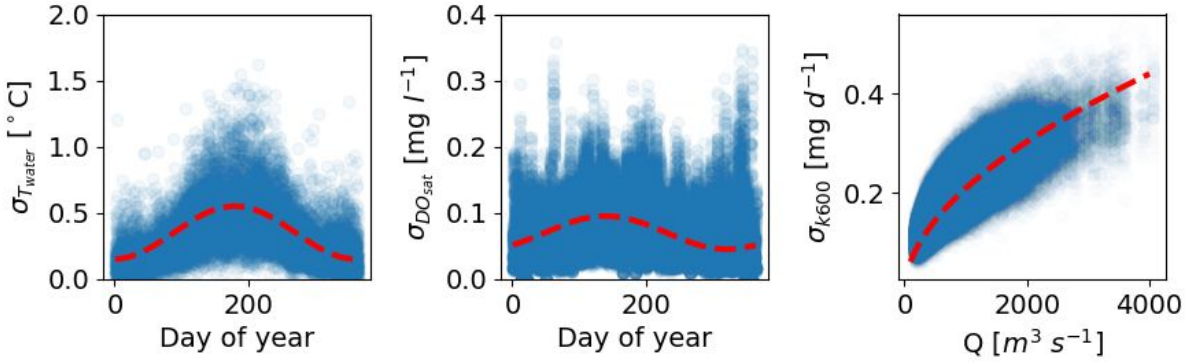

Figure S9: Estimated (blue circles) and modeled (red dashed lines) daily standard deviations of the parameters Twater, DOconc and k600.

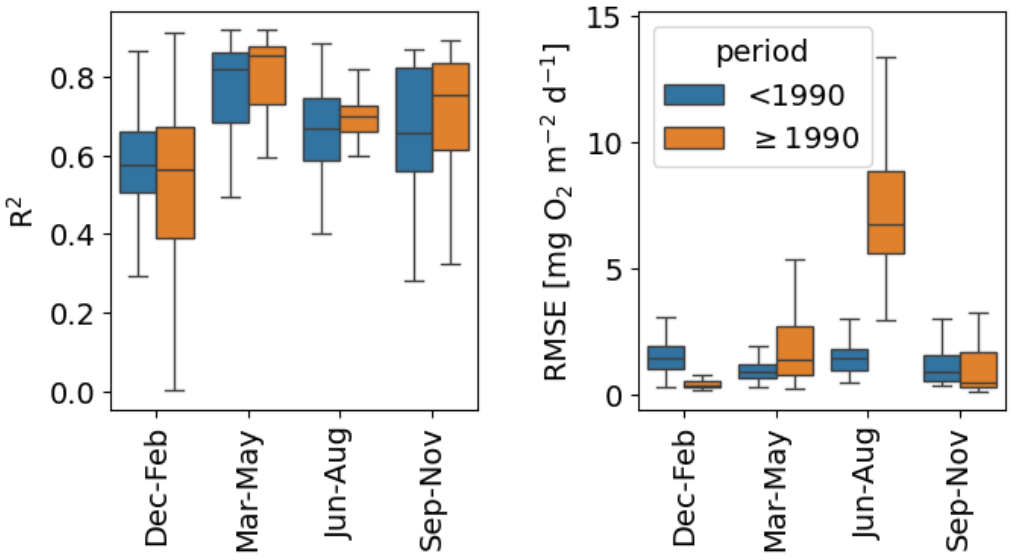

Figure S10: Correlation coefficient R2 (left) and root mean square error (right) for simulated vs. observed dissolved oxygen concentrations, considering seasons and periods (before or after 1990).

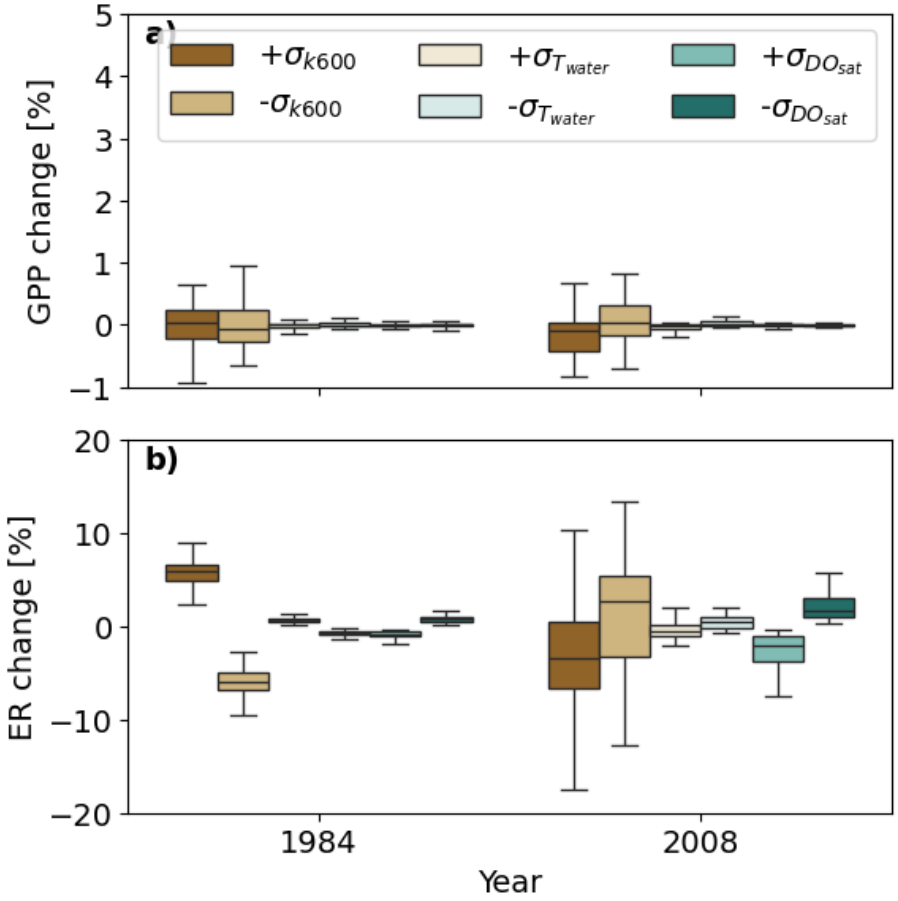

Figure S11: Results of the simplified one-factor-at-a-time sensitivity analysis. a) shows how changes in the parameter Twater, k600 and DOsat affect GPP rates. b) shows the change in ER rates for the same parameter changes. Parameters have been increased or decreased by one standard deviation for each day of the years 1984 and 2008.

S6. Tables

Table S1. The goodness of fit metrics for different approaches of travel time corrections of the water quality time series. For the first three approaches, the outlet time series was shifted by n days as indicated. For the last approach, the travel time estimations were used to determine which shift (1 or 2 days) had to be applied. The root mean square error (RMSE), mean absolute error (MAE), and correlation coefficient R^2 were then computed by comparing the discharge in- and outflows.

	RMSE [m^3/s]	***MAE [m^3/s]***	***R^2***
0-day shift	73	44	0.99
1-day shift	53	33	0.99
2-day shift	66	38	0.99
τ-based shift	108	63	0.97

S7. References

- Aberle, J., Nikora, V., Henning, M., Ettmer, B., and Hentschel, B.: Statistical characterization of bed roughness due to bed forms: A field study in the Elbe River at Aken, Germany, Water Resources Research, 46, https://doi.org/10.1029/2008WR007406, 2010.

- Arroita, M., Elosegi, A., and Hall Jr., R. O.: Twenty years of daily metabolism show riverine recovery following sewage abatement, Limnology and Oceanography, 64, S77–S92, https://doi.org/10.1002/lno.11053, 2019.

- Booker, D. J. and Dunbar, M. J.: Predicting river width, depth and velocity at ungauged sites in England and Wales using multilevel models, Hydrological Processes, 22, 4049–4057, https://doi.org/10.1002/hyp.7007, 2008.

- Chapra, S. C. and Di Toro, D. M.: Delta Method For Estimating Primary Production, Respiration, And Reaeration In Streams, Journal of Environmental Engineering, 117, 640–655, https://doi.org/10.1061/(ASCE)0733-9372(1991)117:5(640), 1991.

- Correa-González, J. C., Chávez-Parga, Ma. del C., Cortés, J. A., and Pérez-Munguía, R. M.: Photosynthesis, respiration and reaeration in a stream with complex dissolved oxygen pattern and temperature dependence, Ecological Modelling, 273, 220–227, https://doi.org/10.1016/j.ecolmodel.2013.11.018, 2014.

- Gao, B.: NDWI—A normalized difference water index for remote sensing of vegetation liquid water from space, Remote Sensing of Environment, 58, 257–266, https://doi.org/10.1016/S0034-4257(96)00067-3, 1996.

- Hall, R. O., Tank, J. L., Baker, M. A., Rosi-Marshall, E. J., and Hotchkiss, E. R.: Metabolism, Gas Exchange, and Carbon Spiraling in Rivers, Ecosystems, 19, 73–86, https://doi.org/10.1007/s10021-015-9918-1, 2016.

- Kamjunke, N., Rode, M., Baborowski, M., Kunz, J. V., Zehner, J., Borchardt, D.,

and Weitere, M.: High irradiation and low discharge promote the dominant role of phytoplankton in riverine nutrient dynamics, Limnology and Oceanography, n/a, https://doi.org/10.1002/lno.11778, 2021.

- Modi, P., Revel, M., and Yamazaki, D.: Multivariable Integrated Evaluation of Hydrodynamic Modeling: A Comparison of Performance Considering Different Baseline Topography Data, Water Resources Research, 58, https://doi.org/10.1029/2021WR031819, 2022.

- Raymond, P. A., Zappa, C. J., Butman, D., Bott, T. L., Potter, J., Mulholland, P., Laursen, A. E., McDowell, W. H., and Newbold, D.: Scaling the gas transfer velocity and hydraulic geometry in streams and small rivers, Limnology and Oceanography: Fluids and Environments, 2, 41–53, https://doi.org/10.1215/21573689-1597669, 2012.

- Richardson, D. C., Carey, C. C., Bruesewitz, D. A., and Weathers, K. C.: Intra- and inter-annual variability in metabolism in an oligotrophic lake, Aquat Sci, 79, 319–333, https://doi.org/10.1007/s00027-016-0499-7, 2017.

- Scharfe, M., Callies, U., Blöcker, G., Petersen, W., and Schroeder, F.: A simple Lagrangian model to simulate temporal variability of algae in the Elbe River, Ecological Modelling, 220, 2173–2186, https://doi.org/10.1016/j.ecolmodel.2009.04.048, 2009.